MECHANICAL PROPERTIES OF POROUS PNZT POLYCRYSTALLINE CERAMICS

Dipak R. Biswas and Richard M. Fulrath

Materials and Molecular Research Division, Lawrence Berkeley Laboratory
and Department of Materials Science and Mineral
Engineering, University of California,
Berkeley, CA 94720

ABSTRACT

Niobium-doped lead zirconate-titanate (PNZT) was used to investigate the effect of porosity on the mechanical properties of a polycrystalline ceramic. Spherical pores (110-150μm diameter) were introduced by using organic materials in the initial specimen fabrication. The matrix grain size (2-5μm) was kept constant. Small pores (2-3μm diameter) of the order of the grain size were formed by varying the sintering conditions. The effect of porosity on strength was predicted quite well by Weibull's probabilistic approach. The Young's modulus showed a linear relationship with increase in porosity. A decrease in fracture toughness with increase in porosity was also observed. It was found that at equivalent porosities, small pore specimens gave higher strength, Young's modulus and fracture toughness compared to specimens containing large pores. Fracture surface analysis, by scanning electron microscopy, showed fracture originated either at the tensile surface or, at the edge of the specimen.

I. INTRODUCTION

Most polycrystalline ceramic materials contain some porosity after firing. This porosity reduces the mechanical strength considerably and is extremely important where ceramics are used as structural materials. During the past twenty years, a number of studies have been performed to elucidate the effect of porosity on strength[1-8] and Young's modulus.[7]

General relationships are beginning to emerge. Most of these investigations considered only the total porosity and neglected the size and shape of the pores. The volume and size effect of porosity on strength was observed by Hasselman and Fulrath[9] and Bertolotti and Fulrath[10] for a sodium borosilicate glass with artificially introduced spherical pores of various sizes and volume fractions. Bertolotti and Fulrath[10] found that the strength was dependent on both the pore size and the volume fraction of porosity. In the case of porous polycrystalline ceramics, inherent flaws are present as well as pores. The effective flaw size for failure can be considered as the combination of inherent flaws on two sides of the pore plus the pore size. Thus, the effective flaw length will be larger for large pore specimens compared to small pore specimens assuming that the inherent flaws are the same for both cases. Therefore, the large pore specimen will fail at a lower stress level than the small pore specimen. In this study, an attempt has been made to perform a systematic experimental study of the mechanical properties of a well-characterized polycrystalline ceramic containing controlled porosity with variations in the volume fraction of pores and pore size.

II. EXPERIMENTAL PROCEDURE

Preparation of Powders and Fabrication of Specimens

Niobium-doped lead zirconate-titanate (PNZT) ceramic was used in the present study. Its composition was $Pb_{0.99}\square_{0.01}(Zr_{0.52}Ti_{0.46}Nb_{0.02})O_3$, where $\square$ is a lead vacancy. The powders of PbO, ZrO_2, TiO_2 and Nb_2O_5 were milled in a vibratory energy mill for four hours using isopropyl alcohol as a liquid medium, then dried and calcined at 850° for four hours. The calcined powders were then mixed with 5.5 w/o excess PbO, milled for four

hours using isopropyl alcohol and polyvinyl alcohol (as a binder) in water, and then air dried. Two types of porosity were considered in this study. Large spherical pores (110-150μm diameter) of controlled amounts were introduced by mixing with organic materials, cold pressing or isostatic pressing, and then decomposing at 250°C for twelve hours prior to sintering. Sintering was carried out at 1200°C for sixteen hours in one atmosphere pressure of oxygen. Small pores (2-3μm) were generated by varying the sintering conditions; namely, green density, and sintering time and temperature (1100°C to 1150°C for one minute to one hour). In both cases, a packing powder ($PbZrO_3 + ZrO_2$) technique was used to control PbO loss from the specimen during sintering.

Density Measurements

The apparent density of large pore specimens was determined from dry weight (W_D) and suspended weight (W_S) in isopropyl alcohol relative to a nickel metal standard. Calculation of the density of the specimen was made by using the equation

$$\rho_{specimen} = \left[\frac{W_D}{W_D - W_S}\right]_{specimen} x \left[\frac{W_D - W_S}{W_D}\right]_{standard} x \rho_{standard} \qquad (1)$$

where $\rho_{standard}$ is the density of nickel, 8.91 gms/cc. The theoretical density of PNZT ceramic was assumed to be 8.00 gms/cc. The bulk density of small pore specimens was calculated from the dry weight and the dimensions.

Mechanical Property Measurements

Strength of the ceramics at room temperature was measured by using a 4-point bending machine with a 0.75 in. overall span and 0.25 in. inner

span. The specimen dimensions were approximately 1.0 in. x 0.3 in. x 0.05 in.

Young's modulus (E) at room temperature was determined by a sonic resonance technique[11] using rectangular specimens with dimensions of 3.0 in. x 0.25 in. x 0.20 in. Once the exact resonant frequency was obtained, Young's modulus was calculated by using the resonant frequency, dimensions, and mass of the specimen. The resonant frequency used to calculate Young's modulus is theoretically correct only for materials without internal damping. To determine the internal damping, the damping capacity[12] of PNZT ceramics was measured from the width of the half-maximum value of the resonance curve. The value was obtained by finding the resonant frequency at the maximum amplitude and then locating the two frequencies above and below the resonant frequency at which the amplitude decreased to half of the resonant amplitude. Damping capacity δ was calculated from the differences of the two frequencies Δf and the resonant frequency f as

$$\delta = 1.8136 \frac{\Delta f}{f} \qquad (2)$$

Fracture toughness (K_{IC}) of the ceramics was determined by the double torsion method.[13]

After fracturing the specimen, the fracture surfaces were observed by using scanning electron microscopy. In some cases, the "river pattern" (markings on the fracture surface) were traced back to determine the fracture origin.

III. RESULTS AND DISCUSSION

A typical microstructure of PNZT ceramics is shown in Fig. 1. The average grain size for large pore (110-150μm) specimens was 2-5μm; and for

small pore (2-3μm) specimens, 1-3μm.

Strength

The strength of the ceramics containing large spherical pores and small pores is shown in Fig. 2. In the case of large pores, strength decreases rapidly with initial increase in porosity and then levels off at about 8 v/o porosity. By using Weibull's probabilistic approach to brittle strength, the experimental results were analyzed and it was found[14] that the strength depends only on the total porosity. However, in the case of small pores, Weibull's approach is not applicable. The experimental results follow a simple model of decreasing cross-sectional area with increasing porosity up to about 5 v/o. The strength values up to 8 v/o of small pores shows a higher value compared to specimens containing large pores. The bending strength is directly related to the load at the point of fracture. For small pore specimens, failure occurs at a higher stress and the load at fracture is higher compared to large pore specimens. This behavior is attributed to the postulate that the small pore specimens contain smaller effective critical flaws that cause failure than the flaws in the large pore specimens.

Young's Modulus

The experimental results for Young's modulus are shown in Fig. 3. The linear relationship

$$E/E_o = 1-KP \qquad (3)$$

describes the experimental data for large pore specimens. E_o was found to be 11.0×10^6 psi with a value of 2.5 for K. For the same pore content, Young's modulus for the small pore material appears to be slightly higher.

The plot of damping capacity against the volume percent of porosity is shown in Fig. 4. Damping capacity shows an increase with increase in porosity. A similar trend was observed by Marlowe and Wilder[15] in case of polycrystalline yttrium oxide. An interesting observation in Fig. 4 is that for small pores, the damping capacity is approximately one third that of the large pore specimens. It is even less than the extrapolated damping capacity value for zero porosity.

In fabricating the specimens, the starting powder (PNZT + 5.5 w/o excess PbO) was the same for all series, but in the case of small pore specimens, mainly the sintering temperature and time were varied to generate different amounts of porosity. The excess PbO forms a lead oxide rich liquid at about 890°C. In sintering large pore specimens at 1200°C for sixteen hours, it is expected that most of the excess PbO evaporates to the packing powder. In the case of small pore specimens which are fired at 1100°-1150°C, it is suspected that some PbO rich liquid remains and is converted during cooling to crystalline PbO and PNZT along the grain boundaries. Thus, the grain boundary structure for small pore specimens may be different resulting in a more continuous PNZT matrix. Therefore, the dissipation of energy will be less for the small pore specimens, as observed, which is reflected in a low damping capacity.

Fracture Toughness

The experimental results for fracture toughness are shown in Fig. 5. K_{IC} decreases with increase in porosity (110-150μm); and a small pore (2-3μm) specimen shows a slightly higher value. By definition, the strength, σ_f, is proportional to K_{IC}; the higher strength for small pore specimens would correspond to a higher fracture toughness, as observed in Fig. 5.

As mentioned, the critical flaw size for small pore specimens is smaller than that for large pore specimens. The flaw size "a" has been calculated from the experimental results using the Griffith-Irwin relationship:

$$a = f(Z/Y)(K_{IC}/\sigma_f)^2 \qquad (4)$$

Where Z is the flaw shape parameter and Y is a geometrical constant. At an equivalent porosity (~4.8v/o), when the K_{IC} value is taken from Fig. 5 and the σ_f value is taken from Fig. 2, it is found that the critical flaw size of large pore specimens is about one and a half times larger than for small pore specimens assuming that f(Z/Y) is the same in both cases. Therefore, the strength of small pore specimens (4.8 v/o porosity) should be expected to be about 1.25 times higher than for large pore specimens. This agrees quite well with the experimental results shown in Fig. 2. The flaw size calculated from K_{IC} and σ_f values is an appreciable fraction of the specimen thickness. Similar results have also been obtained for rock and chalk. Such a large flaw was not detected by conventional electron microscopy. Thus, there must be some uncertainties in interpreting the calculated values as the actual critical flaw size for brittle materials.

Fractographic Analysis

Intergranular fracture was the primary fracture mode with some transgranular fracture observed at high magnification. By tracing back the river pattern, it was found that the fracture originates either at or near the tensile surface, or at the edges of the tensile surface of the specimen. To determine the edge effect on the strength, three highly dense specimens were fabricated by the same processing technique and then

were cut into thin slices for strength measurement. In one-third of the specimens the edges were carefully rounded by using a rotating diamond wheel and polished by using 0.3μm Al_2O_3. For another third of the specimens, after rounding and polishing the edges, the tensile surface was polished. The final third of the specimens were tested in the as-cut condition. Insignificant differences in strength were observed between the three types of specimens. By examining the fracture surface, it was found that the edge failure could be eliminated by rounding off the edges, as shown in Fig. 6. Fracture from the tensile surface could also be minimized by polishing the tensile surface (Figs. 6 b and d).

IV. CONCLUSION

Polycrystalline niobium-doped lead zirconate-titanate ceramics, with small pores, exhibited a higher strength and fracture toughness and slightly higher Young's modulus, than the same material with large pores at equivalent porosity. The higher strength of the small pore specimens is attributed to the smaller effective flaw size that causes failure. Because the strength is proportional to the fracture toughness, the fracture toughness for small pore specimens is higher than for large pore specimens, as observed. Edge failures in bend specimens are eliminated by rounding off the edges.

ACKNOWLEDGEMENTS

The authors would like to acknowledge Professors D. P. H. Hasselman, J. A. Pask and I. Finnie for their helpful comments and suggestions. Discussions with J. Wallace is also acknowledged. Thanks are extended to Richard Lindberg for Scanning Electron Microscopy, Gloria Pelatowski for drafting and Gay Brazil for typing this report. This work was supported by the U.S. Energy Research and Development Administration.

REFERENCES

1. M. Y. Bal'shin, Powder Metallography (in Russian); Metallurgizdat, Moscow (1948).

2. E. Ryshkewitch, "Compression Strength of Porous Sintered Alumina and Zirconia," J. Am. Ceram. Soc., 36 [2], 65-68 (1953).

3. W. Duckworth, "Discussion of Ryshkewitch Paper," Ibid., (2) 68 (1953).

4. R. L. Coble and W. D. Kingery, "Effect of Porosity on Physical Properties of Sintered Alumina," Ibid., 39 (11) 377-85 (1956).

5. F. P. Knudsen, "Dependence of Mechanical Strength of Brittle Polycrystalline Specimens on Porosity and Grain Size," Ibid., 42 (8) 367-87 (1959).

6. E. M. Passmore, R. M. Spriggs and T. Vasilos, "Strength-Grain Size - Porosity Relations in Alumina," Ibid., 48 (1) 1-7 (1965).

7. J. E. Bailey and N. A. Hill, "The Effect of Porosity and Microstructure on the Mechanical Properties of Ceramics," Proc. Brit. Ceram. Soc., No. 15, 15-35 (1970).

8. S. C. Carniglia, "Working Model for Porosity Effects on the Uniaxial Strength of Ceramics," J. Am. Ceram. Soc., 55 (12) 610-18 (1972).

9. D. P. H. Hasselman and R. M. Fulrath, "Micromechanical Stress Concentrations in Two-Phase Brittle-Matrix Ceramic Composites," Ibid., 50 (8) 399-404 (1967).

10. R. L. Bertolotti and R. M. Fulrath, "Effect of Micromechanical Stress Concentrations on Strength of Porous Glass," Ibid., 50 (11) 558-562 (1967).

11. D. P. H. Hasselman, "Tables for the Computation of Shear Modulus and Young's Modulus of Elasticity from the Resonant Frequency of Rectangular Prisms," Applied Research Branch, Research and

Development Div., The Carborundum Co., Niagara Falls, NY (1961).

12. D. R. Biswas, "Influence of Porosity on the Mechanical Properties of Lead Zirconate-Titanate Ceramics," Ph.D. Thesis, University of California, Berkeley, CA 94720 (LBL-5479) (1976).

13. D. P. Williams and A. G. Evans, "A Simple Method for Studying Slow Crack Growth," J. Test Eval., 1 (4) 264-70 (1973).

14. O. Vardar, I. Finnie, D. R. Biswas and R. M. Fulrath, 'Effect of Spherical Pores on the Strength of Polycrystalline Ceramics," Int. J. of Fracture, 13 (2), April (1977).

15. M. O. Marlowe and D. R. Wilder, "Elasticity and Internal Friction of Polycrystalline Yttrium Oxide," J. Am. Ceram. Soc., 48 (5) 227-233 (1965).

FIGURES

1. Microstructure of PNZT ceramics (with 5.5 w/o excess PbO in starting mixture showing (a) spherical porosity, 4.9 v/o and 110-150μm pore size, (b) grain size distribution in nearly theoretically dense specimen, and (c) grain and pore distributions in PNZT-small pore (4.8 v/o) specimen.
2. Porosity dependence of strength of PNZT ceramics containing spherical pores and small pores versus the volume percent of porosity.
3. Young's modulus of polycrystalline PNZT ceramics as a function of volume percent of porosity.
4. Damping capacity of polycrystalline PNZT ceramics as a function of volume percent of porosity.
5. Dependence of room temperature fracture toughness of polycrystalline PNZT on porosity.
6. Fracture surfaces of the PNZT specimens after rounding the edges showing the fracture origin (a and c) from the tensile surface, (b and d) from beneath the polished tensile surface.

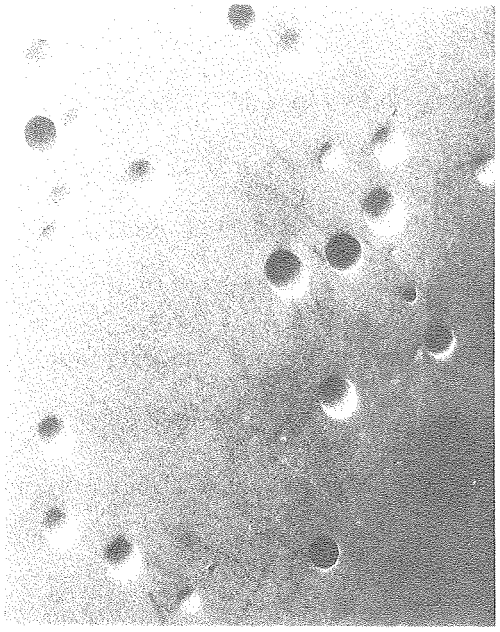

200μ

(a)

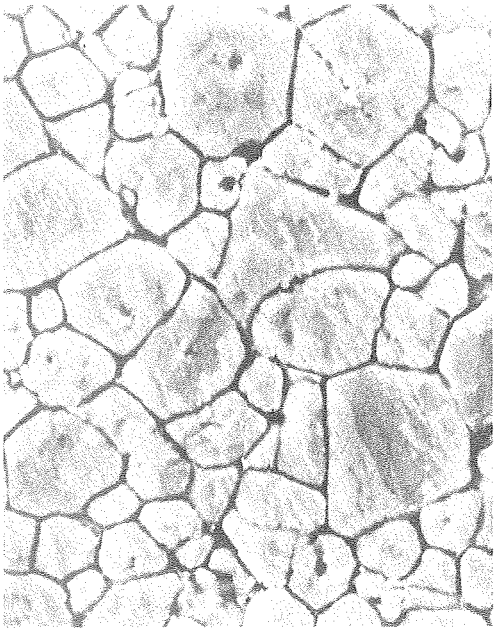

2μ

(b)

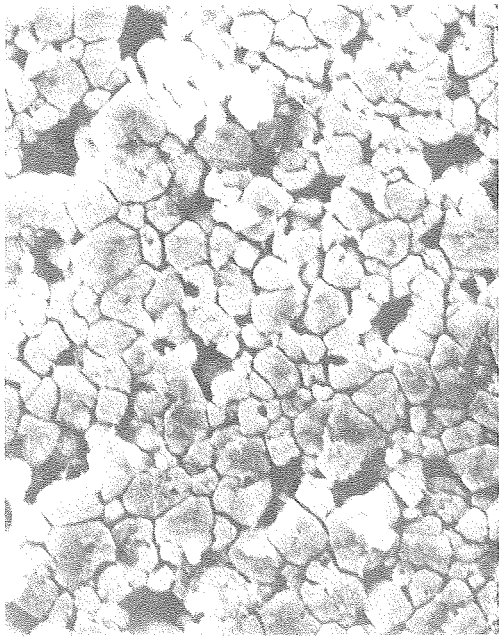

2μ

(c)

XBB766-5596

Fig. 1

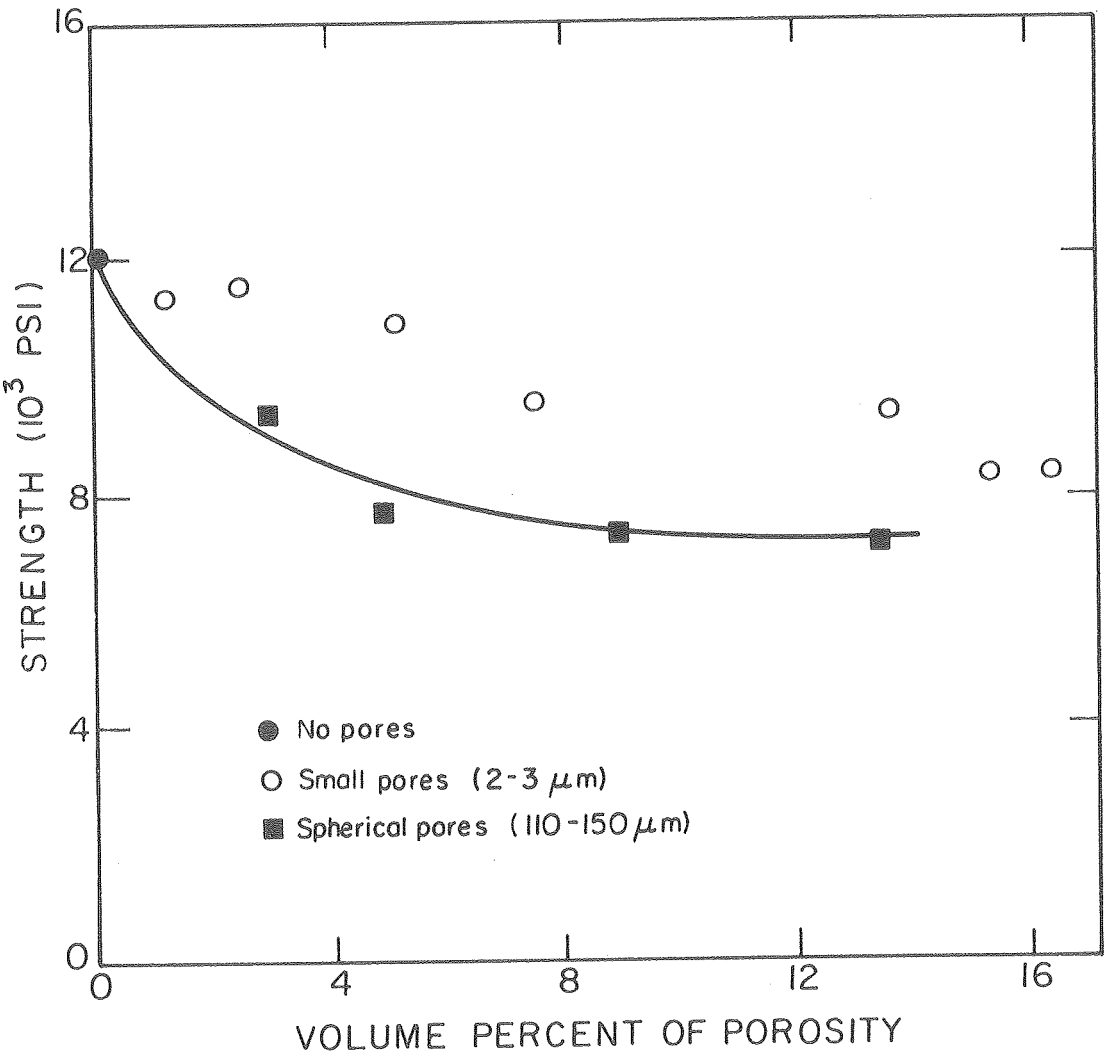

Fig. 2

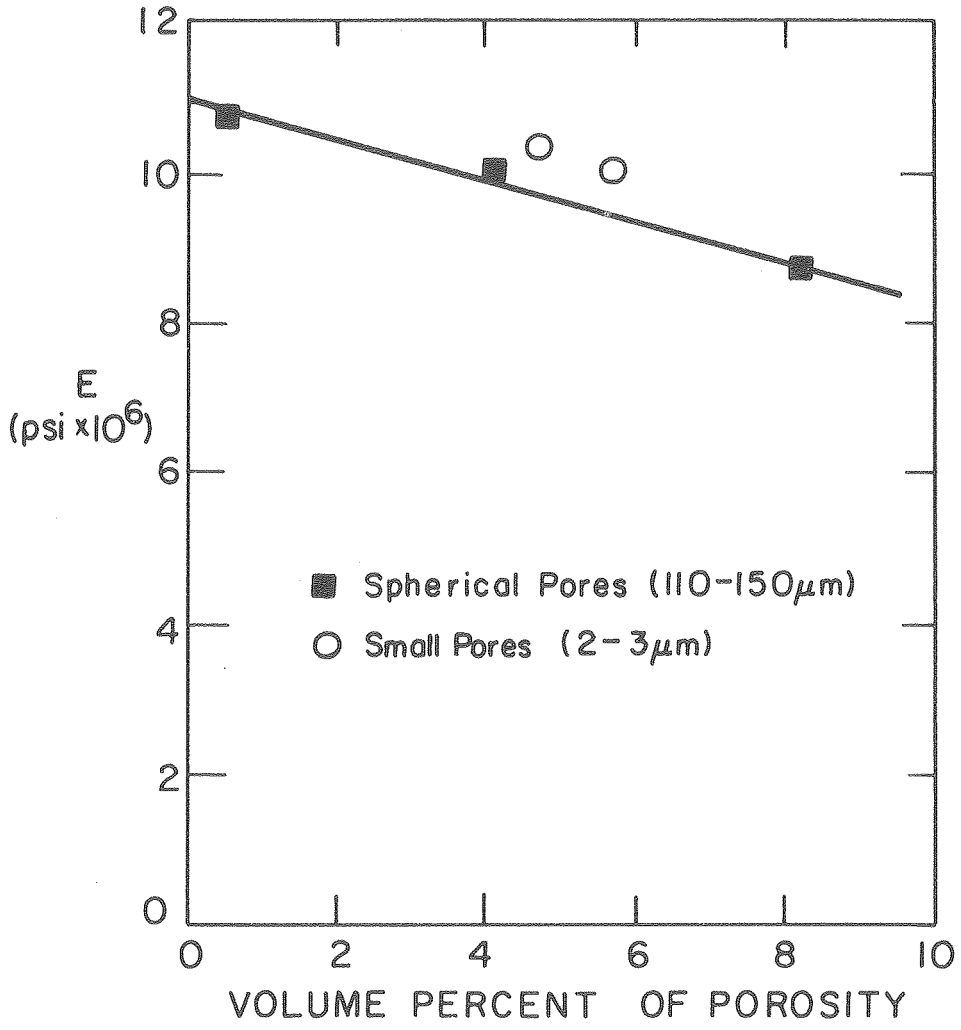
12
10
8
6
4
2
0
E
(psi x10^6)
Spherical Pores (110-150μm)
Small Pores (2-3μm)
0
2
4
6
8
10
VOLUME PERCENT OF POROSITY

Fig. 3

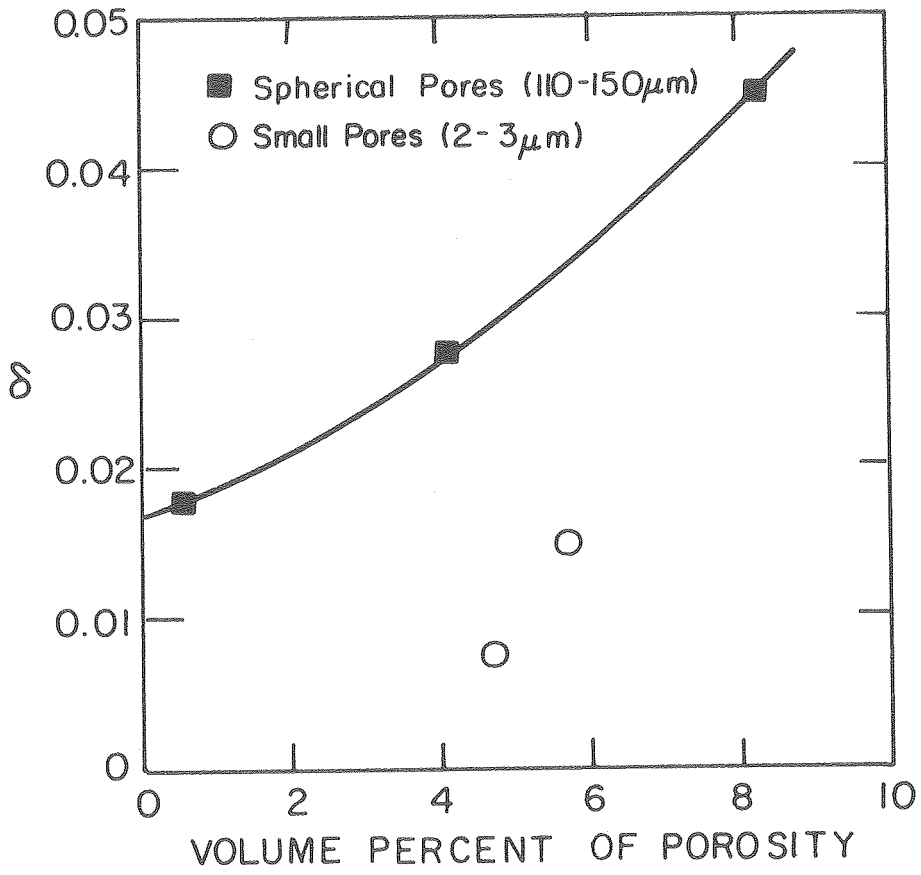

Fig. 4

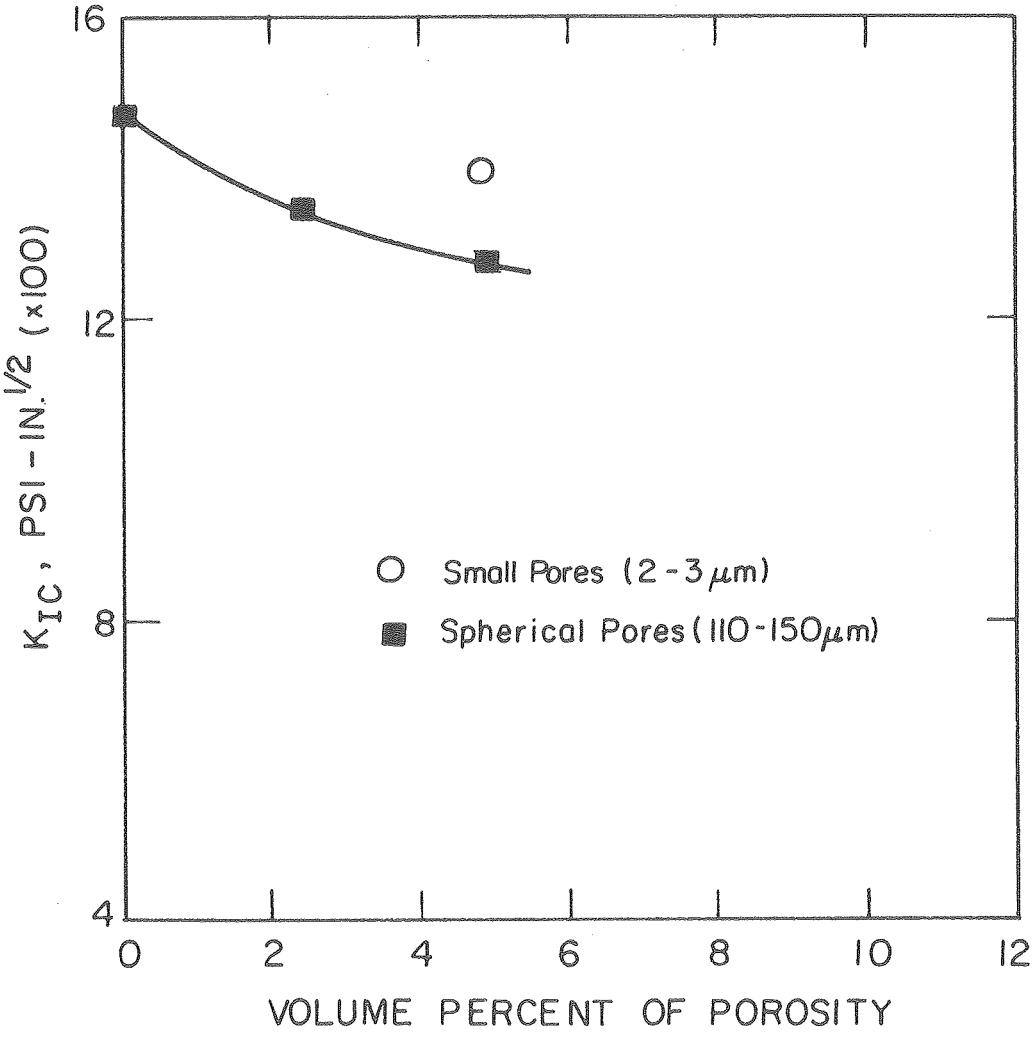
16
12
8
4
0
2
4
6
8
10
12
K_{IC}, PSI - IN.$^{1/2}$ (×100)
VOLUME PERCENT OF POROSITY
Small Pores (2 - 3 μm)
Spherical Pores (110 - 150 μm)

Fig. 5

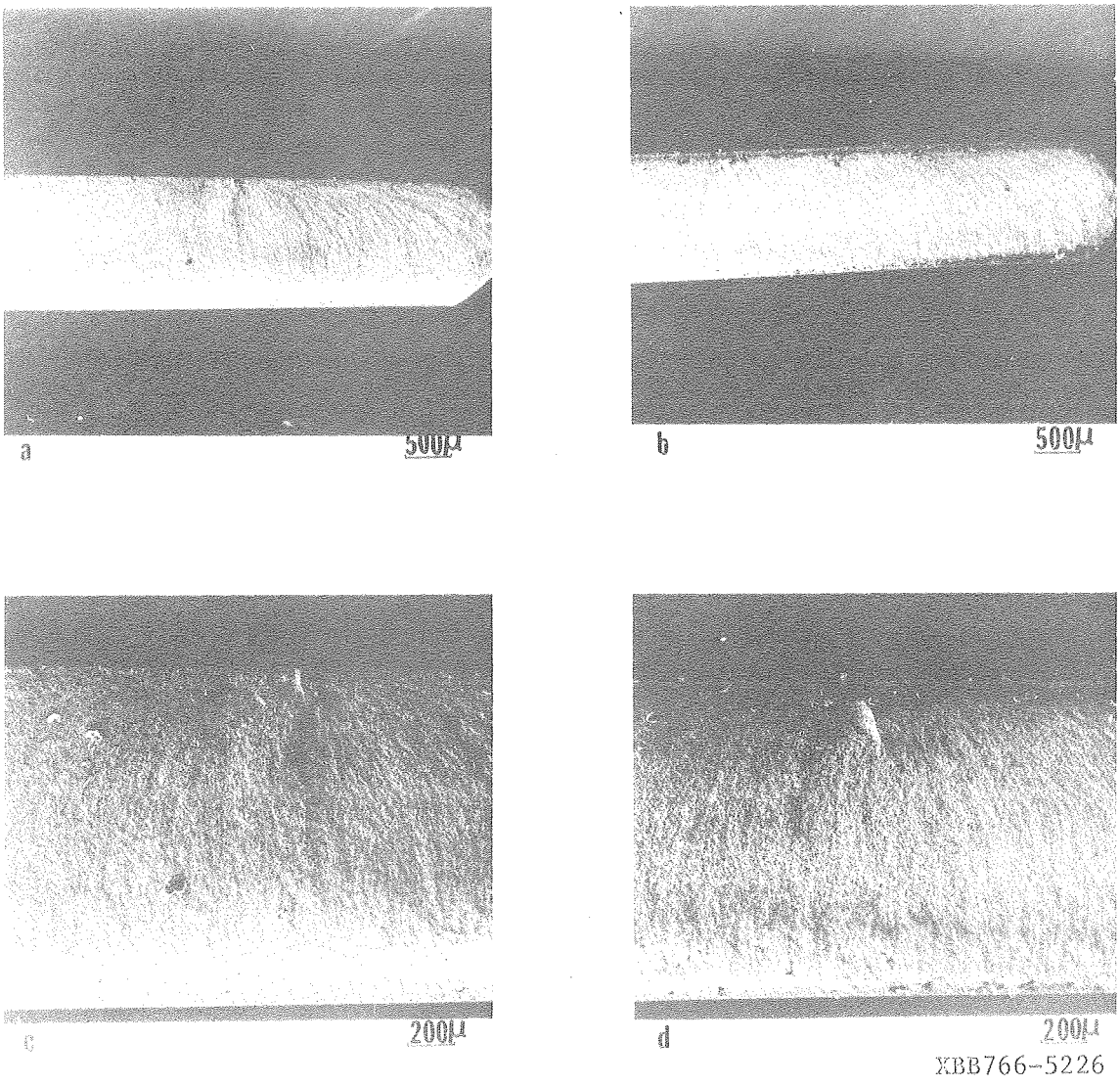

XBB766-5226

Fig. 6

This report was done with support from the United States Energy Research and Development Administration. Any conclusions or opinions expressed in this report represent solely those of the author(s) and not necessarily those of The Regents of the University of California, the Lawrence Berkeley Laboratory or the United States Energy Research and Development Administration.